International Journal of Biomedical and Clinical Sciences
Vol. 5, No. 2, 2020, pp. 75-86
http://www.aiscience.org/journal/ijbcs

Multifractal Segmentation Analysis of Optical Coherence Tomography Angiography Images for Normal and Diabetic Retinopathy Eyes

Gomaa El Damrawi[1, *], Tarek Mohsen[2], Mohsen Zahran[3], El Shaimaa Amin[4]

[1]Glass Research Group, Physics Department, Faculty of Science, Mansoura University, Mansoura, Egypt
[2]Ophthalmology Canter, Faculty of Medicine, Mansoura University, Mansoura, Egypt
[3]Physics Department, Faculty of Science, Mansoura University, Mansoura, Egypt
[4]Physics Department (biophysics), Faculty of Science, Mansoura University, Mansoura, Egypt

Abstract

For normal subjects and diabetic patients, the purpose of this analysis is to measure the blood vascular network density of the retina in the superficial layer using OCTA image technique. Several techniques were applied to the images, such as box counting size, information dimension, lacunarity parameters, and multi-fractal analysis. There were small variations in fractal dimension of retinal vascular network between the images of normal subjects and diabetic patients. The main point of this research is the reliable anatomized segmentation of the vessel and the retinal vascular which analyzed as a multifractal object. The obtain images were then equally divided into several divided regions, with each area being evaluated as an image. The findings were consistent and help us to differentiate between ordinary and diabetes patients. The applied technique of practical analysis is used to describe and characterize images representing complex anatomical structures. However, the fractal dimension measurement as a key index is deeply based on the quality of the images obtained. Furthermore, the selected segmentation methods and the method for measuring the fractal dimension have been standardized.

Keywords

Blood Vascular Network, Optical Coherence Tomography Angiography, Box Counting, Multifractal

Received: February 11, 2020 / Accepted: March 5, 2020 / Published online: April 7, 2020

1. Introduction

Many image processing and analysis techniques have been introduced over the last decades in order to identify the retinal pathologies. Diabetic retinopathy is the most common disease causing in some cases vision loss due to hyperglycemia, which facilitates systemic and functional alternation of the retinal capillary [1, 2]. The angiogenic factors produced by spindle cells promote the growth of new retinal blood vessels (neovascularization) [3]. The diagnostic tools can be categorized either by invasive or non-invasive imaging techniques. Fluorescein Angiography (FA) and Indocynine Green Angiography (ICGA) involves intravenous dye administration and visualization for up to 10-30 minutes. While FA is currently the gold standard for evaluating retinopathy vasculature as it provides 2D images that enable dynamic visualization of blood flow through retinal vessels. FA has some disadvantages as coloring poses risks ranging from nausea to allergic reactions, time consuming and cannot be repeated in the same day. The other one is Swept Source Optical Coherence Tomography Angiography (SS-OCT). It is the latest non-invasive imaging technique [4, 5] that relies on tunable laser scans with a sequential range of wavelengths in just a few seconds. It can provide higher image speeds, resolution and longer image range than Spectral Domain OCT (SD-OCT) [6, 7] for all the vascular layers (superficial

* Corresponding author
E-mail address: gomaaeldamrawi@gmail.com (G. El Damrawi)

layer, deep capillary networks and chroriocapillaries) that were not identified on FA [6, 7]. SS-OCTA uses motion contrast imaging process and works by comparing repeatedly acquired B-scans at a given retinal location caused by erythrocyte movement in retinal vessels, which can then be simply computed and displayed. OCTA can also be performed on the same day several times in succession.

Some of previous studies [7, 8] were conducted using OCTA as a qualitative diagnostic study and others were satisfied with the quantitative analysis of FAZ pixel count and blood vessel density. As a consequence, this study is based on the use of a computer segmentation to identify variations in the complexity of vessel image distribution. In fact, the retinal blood vessel structure branching pattern resembles fractal, i.e. retinal structures do not have a single length scale. Generally, biology is the most important field for the application of fractal concepts because structures of very complex and irregular forms cannot be understood using Euclidean geometry or traditional methods at multiple hierarchical levels. Since fractal geometry identifies the morphogenetic (anatomical) laws of complex structure, retinal diseases can be diagnosed with mathematical modelling of blood vessel information.

Recent studies utilizing fractal modelling of retinal layer structures in virtual picture simulation provide some useful insights into early detection and treatment of retinal diseases. So, our aim is to examine in some depth the early stages of diabetic retinopathy without invasive techniques. The latter, will give us the opportunity to produce fractures and to decode them. Medical photographs that depict anatomically complex structures could in several instances be represented and categorized by fractal analysis.

2. Methods

The retrospective observational case series was approved in (Ophthalmology Center in Mansoura University-Egypt). Around 30 eyes of healthy 35 eyes of diabetic retinopathy subjects were included in this study. The subjects were between 20 to 60 years old. The extent of diabetic retinopathy (DR) was determined via clinical examination by retinal specialist. The normal eyes which were required by staff, visitors and researchers were also evaluated by a retinal specialist and had no chorioretinal diseases.

2.1. Study Design

All subjects underwent imaging on (Triton Top-Con Swept-Source OCTA). The device has acquisition speed of 100,000 A-scans/sec with 1050 nm wavelength, B-scan acquisition approx. 0.01 sec, and 3D scan acquisition time approx. 0.65 sec. Imaging was performed using angiographic 3*3 nm scan pattern consist of 5 repeated B-scans of 500 A-scans each at 500 raster positions, centred at the fovea centre.

2.2. The OCTA Image Processing

Firstly, the resulted gray-scale images from OCTA are subjected to MATLAB Simulink version 2013 to be cropped, binarized, setting threshold and image processing to enhance the resulted images. Then, use image-J software and Frac-lac plugin to get the satisfactorily results.

2.3. Fractal Analysis

Benoit Mandelbrot's term "fractal" [9] is used to characterize continuous but not differentiable spatial and temporal phenomena [9, 10]. In other words, a fractal geometrically is a rough or fragmented geometric shape that can be subdivided into parts, each of which is at least a copy of the entire or geometric shapes that appear chaotic or irregular compared to those of standard geometry (line, square, sphere, etc.). As is well known, one of the fractals like objects [10, 11] as shown in Figure 1, is the human retinal vascular network. Fractal dimension enables us to measure the degree of complexity by assessing how rapidly our measurements increase or decrease as our scale increases or decreases [14, 15, 16].

Image ID: 2879R

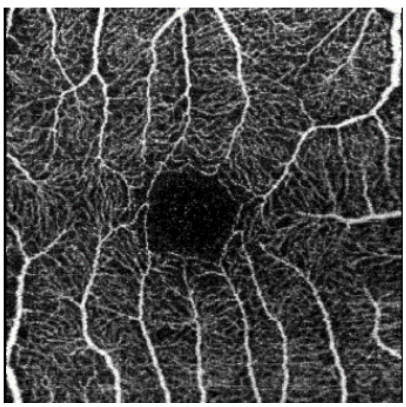

(a)

Image ID: 7933R

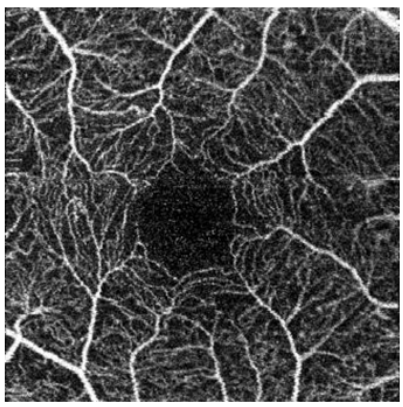

(b)

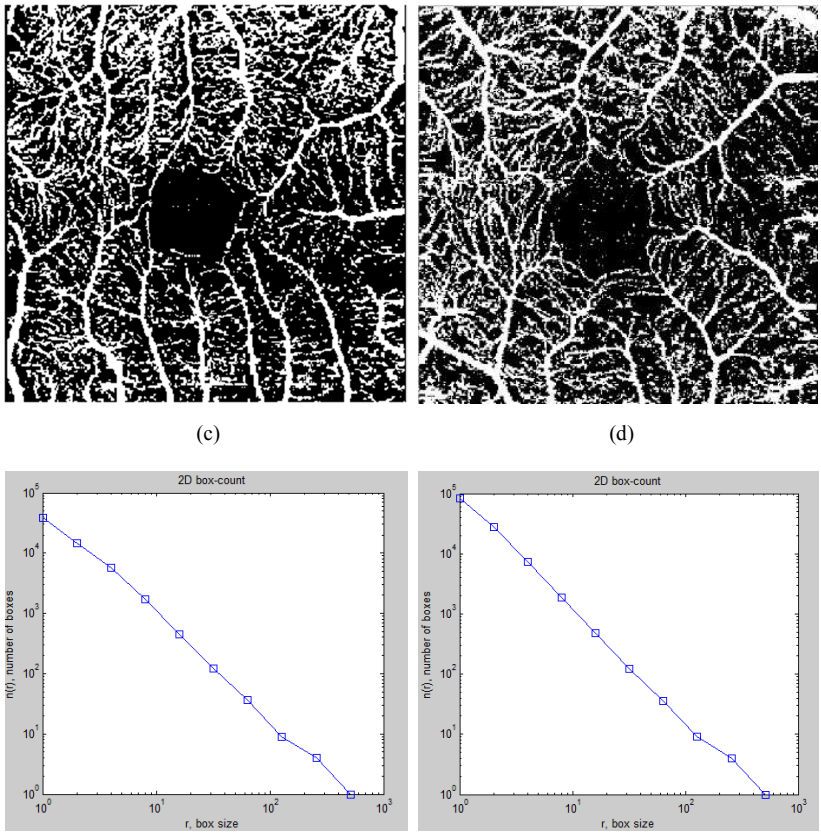

Figure 1. The human retinal vascular network for (a) normal (b) pathological images (c) and (d) the binary processed images (e) and (f) the regression lines of log plot of N(r) versus the log of 1/r for normal and pathological cases respectively.

There are several fractal dimensions calculating methods; the most widely used is box counting due to its simplicity. In order to calculate the box-counting fractal dimension, grids composed of quadrangular boxes with variable side length (r) were superimposed onto the images counting the number of boxes, N(r) occupied by at least one pixel of the image, and recording for box size. The fractal dimension DF is obtained by the slope of the regression line of log plot of N as a function of r versus the log of 1/r

$$DF = \frac{logN(r)}{log(1/r)} \quad (1)$$

The relation between Hurst exponent H and DF given by

$$DF = D_T + 1 - H \quad (2)$$

Where D_T is known as topological dimension and H is very important to characterize Fractional Brownian method.

3. Results and Discussion

The average fractal dimension for normal eyes DF =1.7347 with SD=0.2223 and the average fractal dimension for pathological eyes DF =1.735 with SD=0.2293. From these results, it is found that the values of fractal dimension for normal and pathological eyes are very close to each other, so there is a limitation for using this method to diagnostic. It is surly to confirm that mono fractal approach used as a specific method to study vascular retina geometry suffers from a fundamental problem. The retinal structures do not have the single length scale. Also, the measurement of the fractal dimension as a key index is very sensitive to the quality of the obtained images. In order to solve this difficulty, we turn our attention to what is called multifractal analysis.

3.1. Multifractal and Lacunarity Analysis

There are two problems when dealing with fractal dimension analysis for retinal blood capillaries. First: it describes how much blood capillaries network is filled but doesn't indicate how the it can be distributed. Second, the retinal vessels may have different morphology properties in different regions that lead to an error in computed DF to overall the image, because of the human retinal vessels' structures are geometrical multifractal. In order to overcome these limitations, Mandelbrot [12] introduced lacunarity.

3.2. Lacunarity

Lacunarity is a measure that describes the distribution of sizes of gaps surrounding the object within the image, as it

measures how patterns especially fractals fill space where patterns having more or larger gaps [12, 13]. In case of retina, high lacunarity reflects many blood vessels network sized gaps, and low lacunarity reflects similar sized blood vessels network gaps or little gab variance [14]. The most widely method used to calculate the lacunarity is glinting-box algorithm by Allain and Cloitre [1991]. The lacunarity λ was evaluated using FracLac, there are many λs, one for each size of the sampling unit. The mean lacunarity (or Λ) is usually an average over all sizes used to sample an image was expressed as (Image J software; FracLac V 2.0f for Image J software):

$$\Lambda = \frac{\sum(1+(\sigma/\mu)^2)}{n} \quad (3)$$

Where σ is the standard deviation, μ is the mean for pixels per box at this size, r, in a box count at this orientation and n is the number of box sizes.

3.3. Multifractal Analysis

The main remark from the previous section is, the single fractal dimension is not enough and not precise to describe the system. Therefore, it is useful to consider multifractal when its different regions have different fractal properties. In many cases, multifractal scaling is considered the generalization of simple scaling which represents an important characteristic of many growth phenomena.

There are two methods for computing multifractal spectrum, first: box counting method which based on the same principle as fractal dimension. The image is splitted into different box sizes. While the second method based on wavelet transform, hence the image is used as an oscillating box to be represented. Our concern is to use the box counting methods to study the multifractal analysis of blood vessels using Image J software and Fraclac plugin with the default box sizes. The range of box sizes used for fractal and Multifractal dimensions is 10 pixels as the minimum box size and 100% for maximum box size. Two techniques are used by using image J with Fraclac plugins; they can be summarized as follow:

3.3.1. Generalized Fractal Dimension

The Renyi fractal dimensions or generalized fractal dimension (GFD) [4, 5] are important in studying the non-linear analysis and statistics of medical images as indicators for randomness of blood vessels network in retina. It can be characterized by obtaining generalized dimension D_q, where q is the exponent variable that can express the fractal properties in different image scales [16]. The q ranges between -∞ to ∞ to represent the limits of generalized dimension spectrum, it can be expressed as

$$D_q = \frac{\tau(q)}{(q-1)} \quad (4)$$

with,

$$\tau(q) = \lim_{r\to 0} \frac{\ln \sum_{i=1}^{N} (P_i(r)^q)}{\ln(\frac{1}{r})} \quad (5)$$

Where P_i is the distribution probability and r are the box size.

It was considered in the previous studies that [16], the values D_0, D_1, D_2 are remarkable, in capacity dimension, information dimension and correlation dimension respectively. The plot of D_q versus q is almost a sigmoidal function shape and decreasing in multifractal structure. Therefore, several studies characterize the multifractality status if $D_0 \geq D_1 \geq D_2$ is satisfied. Figure 2 shows the plot of D_q versus q for normal and pathological cases.

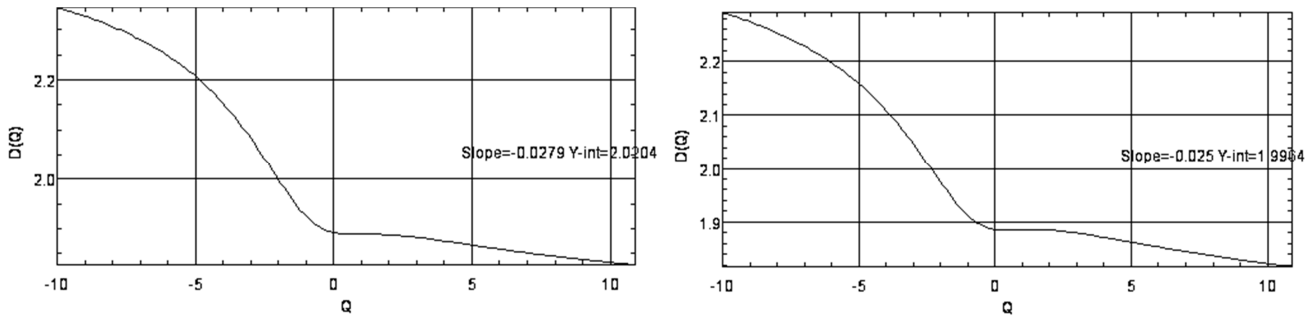

(a) (b)

Figure 2. Plot of D_q versus q for (a) normal and (b) pathological cases.

Figure 2 shows the GFD as an example for all cases for normal and pathological eyes for the retinal superficial blood vessel network. Although the two images for normal and pathological patients, GFD cannot provide us with precise diagnostic information, and the pathological cases' lacunarity is slightly greater than normal eyes. Table 1 summarizes the generalized fractal dimensions for 8 normal and 8 pathological cases with the lacunarity and standard deviations for each image.

Table 1. Generalized fractal dimensions for 16 patient retina images.

Image ID	Status	D_0	σ_0	D_1	σ_1	D_2	σ_2	Lacunarity	σ_Λ
1734R	N	1.902	±0.0665	1.898	±0.0897	1.895	±0.0535	0.2105	±0.0206
2743R	N	1.868	±0.0734	1.86	±0.1035	1.854	±0.0823	0.175	±0.0059
2879R	N	1.892	±0.0691	1.888	±0.091	1.887	±0.0821	0.2841	±0.0245
6961R	N	1.8854	±0.0639	1.874	±0.0918	1.87	±0.0723	0.2098	±0.0069
7031R	N	1.89	±0.0578	1.887	±0.0827	1.885	±0.0646	0.2145	±0.0142
7037R	N	1.883	±0.0675	1.878	±0.0933	1.877	±0.0825	0.1994	±0.0152
12203R	N	1.893	±0.072	1.891	±0.097	1.89	±0.092	0.2353	±0.0216
12203L	N	1.897	±0.0745	1.896	±0.088	1.894	±0.077	0.2238	±0.0278
5730R	P	1.871	±0.0683	1.859	±0.1014	1.853	±0.811	0.2405	±0.0074
5735R	P	1.866	±0.0742	1.848	±0.1018	1.844	±0.0625	0.2429	±0.0048
6004R	P	1.875	±0.08	1.863	±0.106	1.858	±0.088	0.2642	±0.0168
7933R	P	1.886	±0.0593	1.885	±0.082	1.884	±0.0623	0.2754	±0.026
9386R	P	1.887	±0.0662	1.884	±0.0928	1.882	±0.0524	0.3125	±0.0193
10972L	P	1.891	±0.0616	1.884	±0.0912	1.878	±0.0761	0.2411	±0.0181
2190L	P	1.89	±0.0656	1.885	±0.0932	1.88	±0.0765	0.2422	±0.0155
2944L	P	1.911	±0.0691	1.895	±0.1045	1.884	±0.0854	0.3178	±0.0174

N: Normal, P: Pathological

3.3.2. Multifractal Spectrum F(α)

One way to characterize the image function statistics is through multifractal F(α) spectrum (Hausdrouf dimension F(α)) as a function of singularity strength, the function is shown in Figure 3 which describes singularities occurring in considered probability measure.

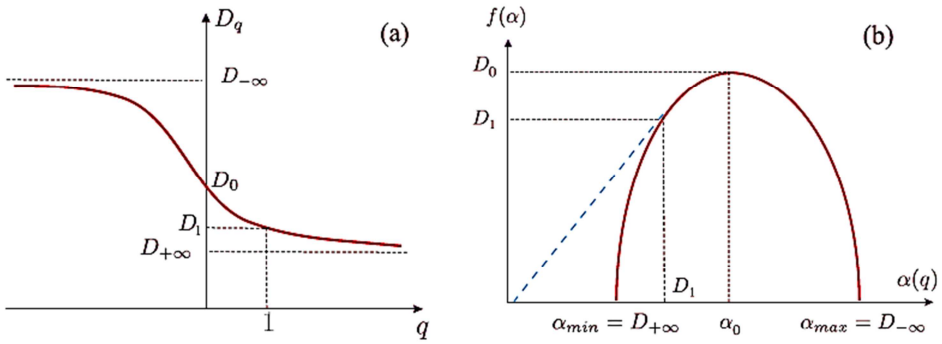

Figure 3. (a) The generalized dimensions D_q as a function of any real q, where $-\infty < q < \infty$, and (b) the singularity multifractal spectrum $f(\alpha)$ versus the singularity strength α.

Figure 3 shows general changes as the maximum value of f (α) is D_0, $f(D_1) = D_1$; and the line joining the origin to the point on the $f(\alpha)$ curve where $\alpha = D_1$ is tangent to the curve.

Let

$$N(\alpha) = L^{-f(\alpha)} \tag{6}$$

Where $N(\alpha)$ represents the number of boxes such that the probability P_i of finding pixels with region i size, L is the box size.

$$P_i = L^{\alpha_i} \tag{7}$$

$F(\alpha)$ is the fractal dimension to all regions with singularity strength between α and α+dα with values between -∞ and ∞ with Legendre transformation as [16].

$$F(\alpha(q)) = q\alpha(q) - \tau(q) \tag{8}$$

Figure 4 shows the f(α) spectrums for different normal and pathological images, that represents the multifractility of retinal blood vessels concavity for both groups. In this case the spectrum is parabola with concavity facing down [17, 18], the singularity spectrum of retinal blood vascular network has the behavior of a multifractal geometry for normal and pathological cases [16]. They have also shown that the retinopathy cases presented lower singularity compared to normal retinas.

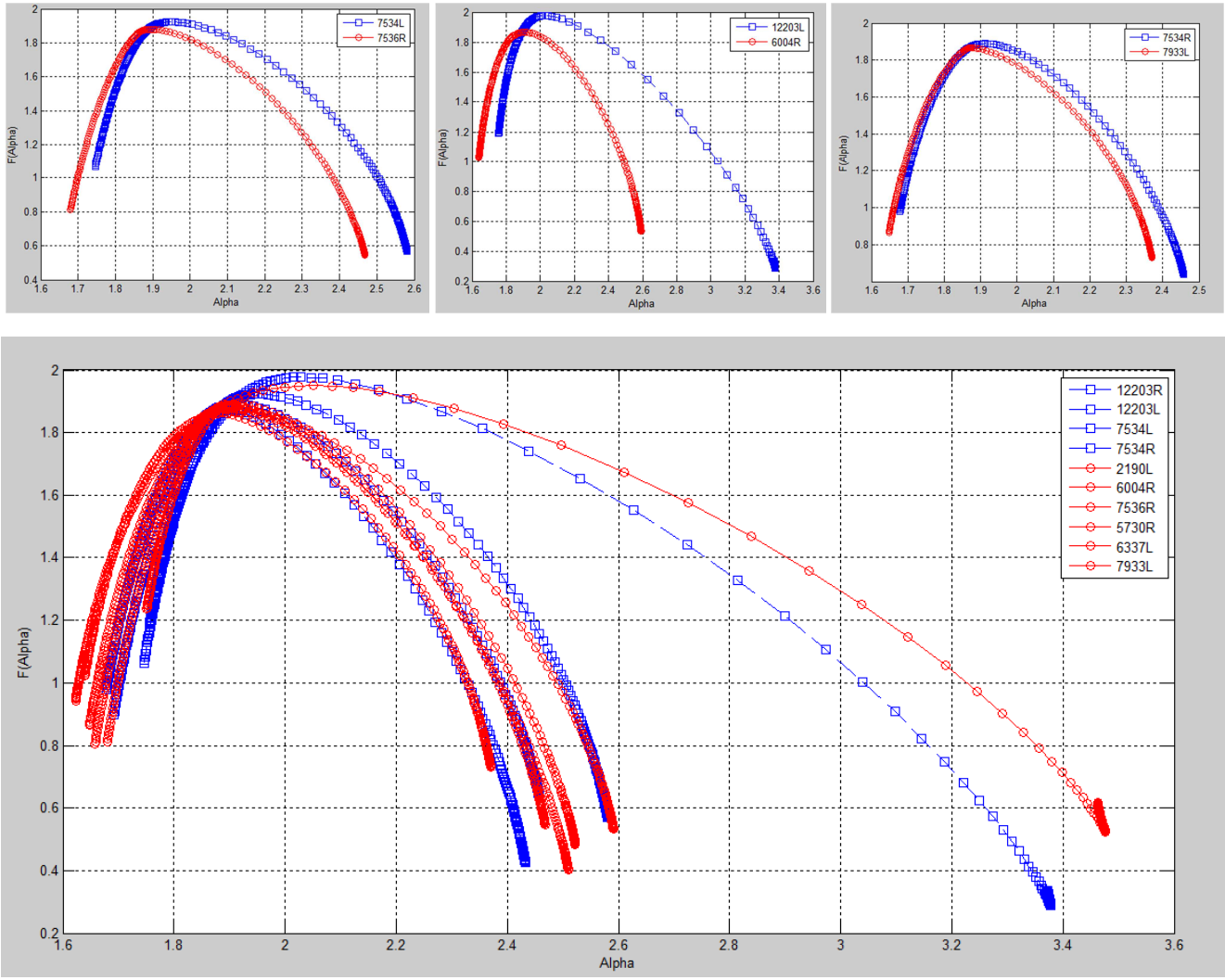

Figure 4. The red circled lines are F(α) spectrum for pathological cases while the blue rectangle lines are the spectrum for normal cases.

From Figure 4 the F(α) spectrum shifted in pathological cases to the left (the lower α range) instead of normal cases, these results can be observed in comparison between normal and pathological cases curves. Our results are in a good agreement with previous research presented in references [6, 7, 17] for STARE database fundus photos that are skeletonized and neglected in the retinal blood vascular network in more detail. Finally, all fractal and multifractal methods used cannot provide us with precise information on normal and pathological cases because some images have different distribution of the blood vessels. Add to this the blood vessels in one part of the image can have a huge distribution while the other parts of the same image have normal distribution. So, finding the image as a whole with a fractal or multifractal dimension cannot provide accurate information. This directly leads us to what is called segmentation of the image.

3.3.3. Multifractal Segmentation

Image segmentation is a good choice for retinal blood vascular network analysis because of the different vessels distributed in the image parts to characterize multifractal spectrum irregularities. The multifractal dimensions and lacuna for the whole images may not provide a precise diagnosis as they converge for normal and pathological images. In addition, in some cases the image has an abnormal distribution of retinal vessels, especially parts not for the image. The solution is to divide the patient's image into 9 segments and studies each differing depending on the location of anomalies in the blood vessels. These nine segments can be identified as superior, superior, supertemporal, nasal, macular, temporal, inferior nasal, inferior, and inferotemporal nasal segments. The following figures 5-8 show various segmented images with results summarized.

Normal Eyes: Left Eye:

1. Id: 12203L

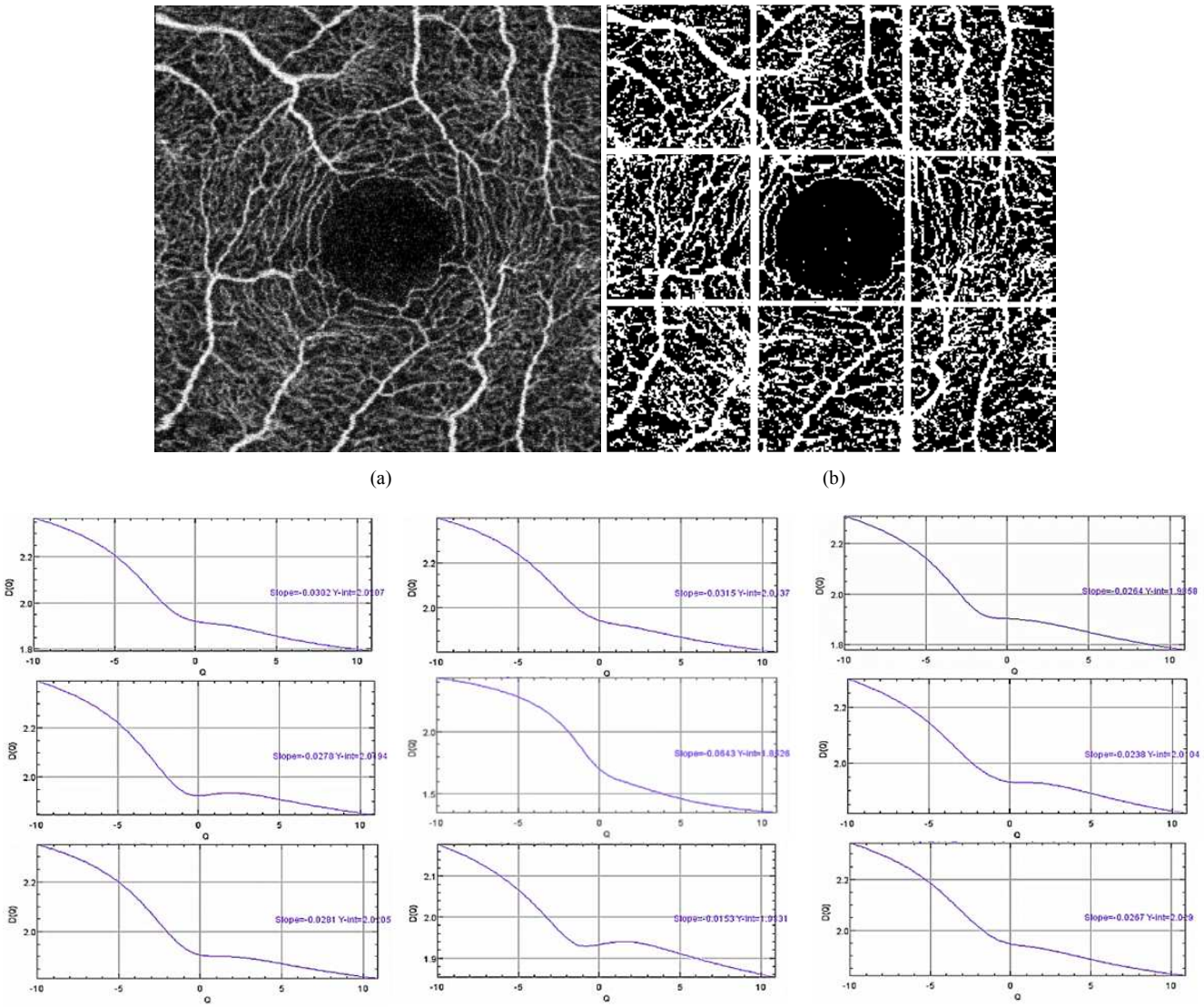

(a) (b)

(c)

Figure 5. Left Normal eye Image with Id: 12203 (a) SWEPT-Source Image (b) binary image (c) multifractal spectrum for each segment.

Table 2. Multifractal Dimensions for image Id: 12203.

Retinal Region	D_{-10}	D_0	D_1	D_2	D_{10}
Whole	2.21	1.911	1.91	1.895	1.855
Nasal superior	2.3676	1.9206	1.9115	1.9029	1.7993
Superior	2.3994	1.9435	1.9276	1.9151	1.811
Superotemporal	2.307	1.903	1.898	1.8904	1.7883
Nasal	2.393	1.924	1.931	1.9354	1.8526
Macular	2.434	1.699	1.622	1.577	1.3583
Temporal	2.302	1.932	1.929	1.926	1.8274
Nasal inferior	2.34	1.907	1.9013	1.899	1.819
Inferior	2.18	1.94	1.939	1.9386	1.861
Inferotemporal	2.342	1.946	1.937	1.928	1.829

Right Eye:

2. ID: 2743 R

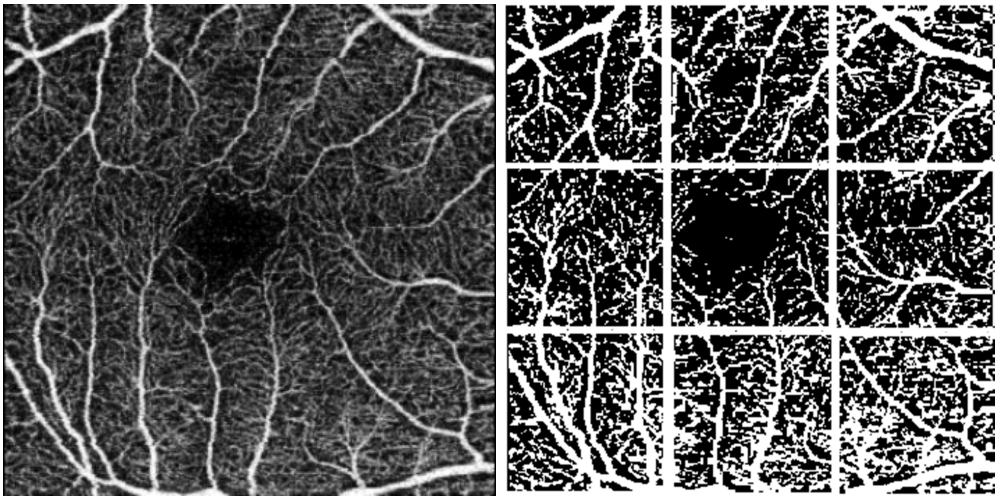

(a) (b)

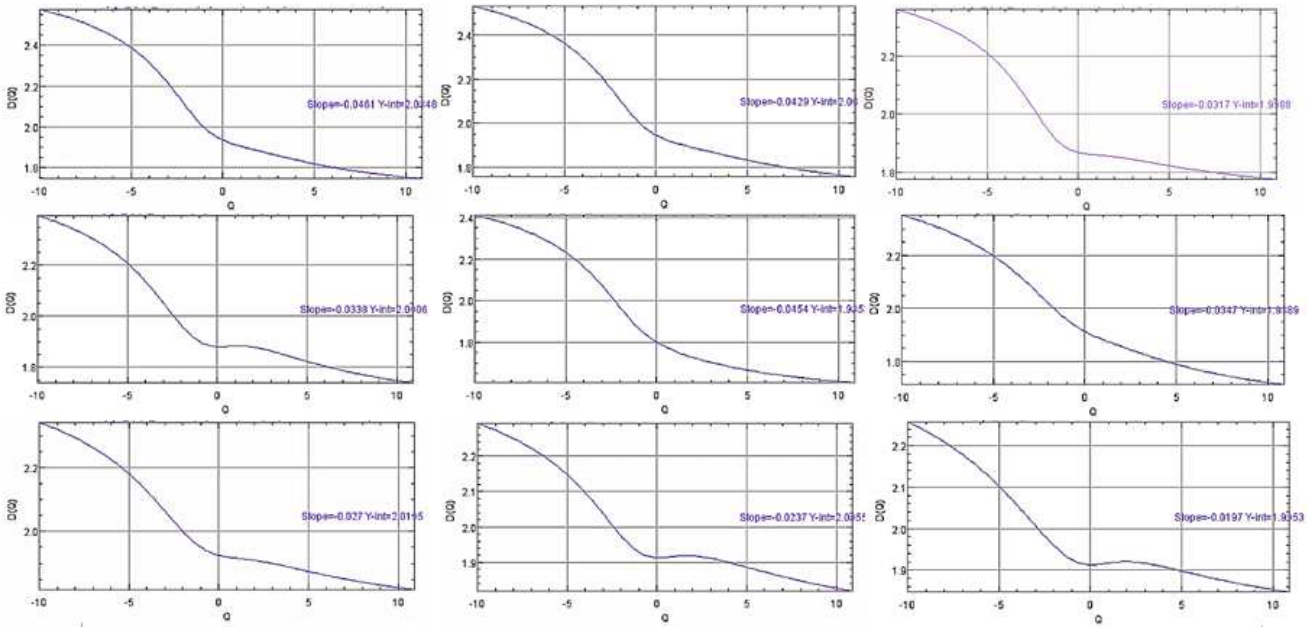

(c)

Figure 6. Right Normal eye Image with Id: 2743 (a) SWEPT-Source Image (b) binary image (c) multifractal spectrum for each segment.

Table 3. Multifractal Dimensions for image Id: 2743.

Retinal Region	D_{-10}	D_0	D_1	D_2	D_{10}
Whole	2.36	1.869	1.86	1.853	1.782
Superotemporal	2.575	1.935	1.905	1.882	1.7542
Superior	2.53	1.947	1.913	1.891	1.767
Nasal superior	2.36	1.868	1.859	1.853	1.782
Temporal	2.47	1.904	1.889	1.879	1.77
Macular	2.412	1.8015	1.7578	1.7272	1.6122
Nasal	2.353	1.913	1.882	1.856	1.7207
Inferotemporal	2.341	1.925	1.916	1.909	1.824
Inferior	2.186	1.883	1.878	1.862	1.711
Nasal inferior	2.31	1.868	1.828	1.799	1.672

Abnormal Eyes:

Left Eye:

Id: 2190L

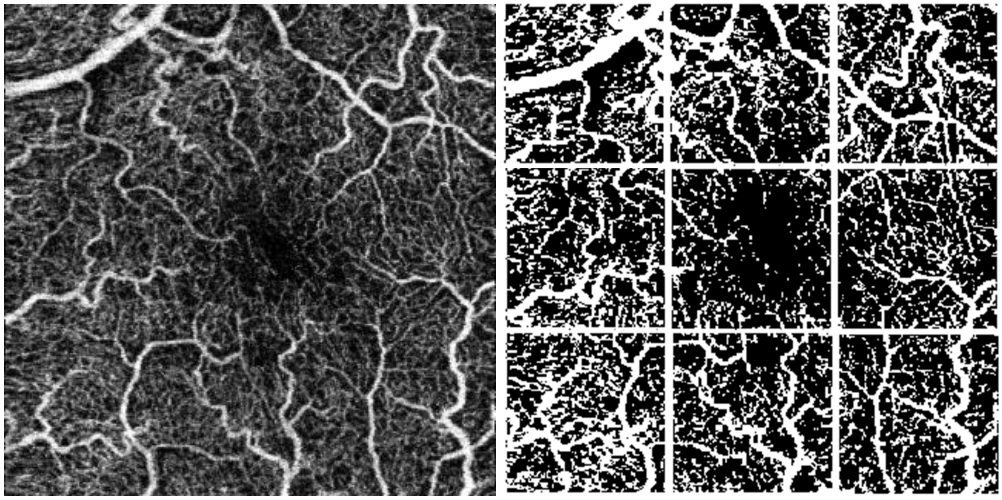

(a) (b)

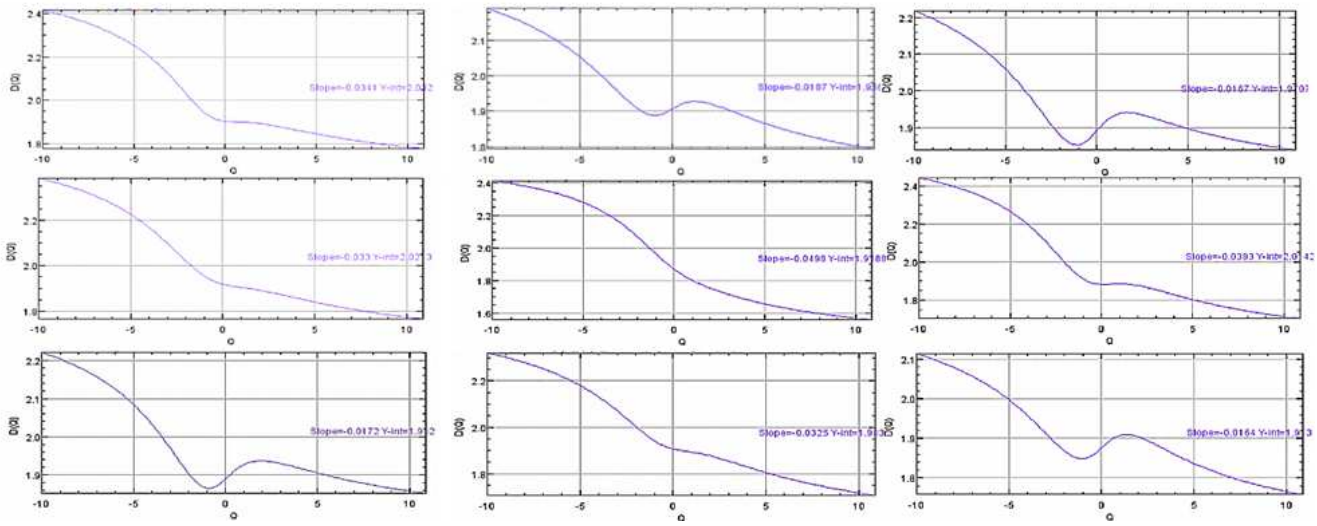

(c)

Figure 7. Left abnormal eye Image with Id: 2190 (a) SWEPT-Source Image (b) binary image (c) multifractal spectrum for each segment.

Table 4. Multifractal Dimensions for image Id: 2190.

Retinal Region	D_{-10}	D_0	D_1	D_2	D_{10}
Whole	2.323	1.891	1.8846	1.878	1.8
Nasal superior	2.415	1.904	1.8995	1.892	1.7875
Superior	2.191	1.907	1.927	1.9217	1.801
Superotemporal	2.218	1.892	1.934	1.94	1.846
Nasal	2.385	1.919	1.9045	1.8922	1.774
Macular	2.414	1.8706	1.802	1.7534	1.569
Temporal	2.443	1.883	1.885	1.876	1.714
Nasal inferior	2.221	1.889	1.927	1.937	1.858
Inferior	2.32	1.907	1.8936	1.877	1.718
Inferotemporal	2.11	1.875	1.907	1.904	1.766

Right Eye:

Id: 6004R

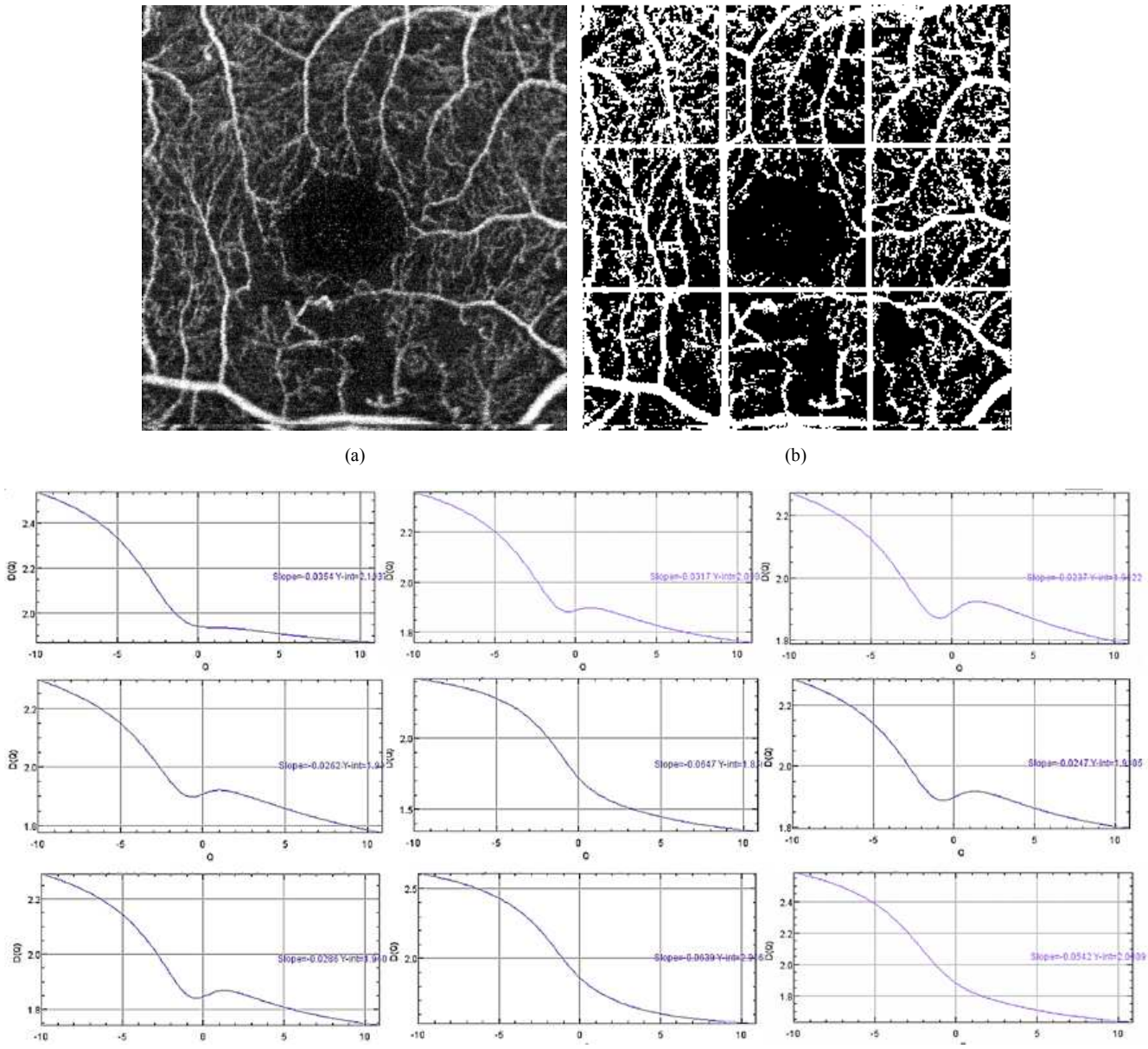

Figure 8. Right abnormal eye Image with Id: 6004 (a) SWEPT-Source Image (b) binary image (c) multifractal spectrum for each segment.

Table 5. Multifractal Dimensions for image Id: 6004.

Retinal Region	D_{-10}	D_0	D_1	D_2	D_{10}
Whole	2.39	1.875	1.863	1.858	1.804
Superotemporal	2.54	1.943	1.937	1.934	1.874
Superior	2.4	1.888	1.899	1.887	1.767
Nasal superior	2.274	1.888	1.9203	1.9222	1.796
Temporal	2.29	1.907	1.921	1.912	1.785
Macular	2.42	1.723	1.621	1.558	1.356
Nasal	2.28	1.895	1.916	1.913	1.8
Inferotemporal	2.29	1.846	1.867	1.863	1.749
Inferior	2.61	1.863	1.773	1.71	1.541
Nasal inferior	2.58	1.881	1.824	1.785	1.639

These indications can encourage changes in vascular architecture that are characteristic of diabetes retinopathy. In this research, we used different methods that could discern the geometric structure of the retinal blood vascular network. The Optical Coherence Tomography Angiography photos are used in place of Fluorescein Angiography [16]. The retinal blood vascular network has a fractal dimension that is larger than 1 and lower than 2 closes to 2 indicating a more complex network especially in OCTA images due to the tiny details observed in these image types, especially 3 * 3 nm scanning pattern than FA images. By using the method of box counting fractal dimensions [19], the results between normal and retinopathic eyes are very close to each other and do not give high diagnostic accuracy. For all cases, multifractal and lacunarity analyzes are applied to the entire image, as lacunarity has the ability to recognize various fractal structures with a close fractal dimension or the same as measuring heterogeneity [13].

For regular and retinopathic situations, the lacunarity and GFD parameters were not statistically different from those in sec. (4.1). Multifractal analyzes do not obtain the results for the entire image, which give the exact diagnosis. The multifractal segmentation method (singularity spectrum) is then applied in all cases, as OCTA images of retinal blood vessels have been binarized and fractionated into nine equal regions following a multifractal analysis by Image J Software (Frac-lac). The condition of generalized dimension that can be described as follows: $D_0 \geq D_1 \geq D_2$ [12, 16, 19] is in agreement with all normal cases images figures 5, 6 and tables 2 and 3. It should be noted, however, that all abnormal cases of diabetic retinopathy images such as figures 7, 8 and tables 4 and 5 deviate from our criterion condition D_0 [D_1] D_2. From these results we can identify the regions indicating early diagnosis of retinopathy in patients with diabetes and the specific damaged regions.

4. Conclusion

The computer image visualization of retinal layers using fractal geometry can provide some insight into early detection and diagnosis of retinal diseases. The most common feature of fractal objects is that they are self-similar in terms of statistical invariance of scale. The fractal analysis is used to describe and characterize images representing complex anatomical structures. Be careful, however, that the fractal dimension measurement as a key index is deeply based on the quality of the images obtained. Furthermore, the selected segmentation method and the method for measuring the fractal dimension must be standardized. The main interest of this work is the reliable anatomized segmentation of the vessel, the retinal vascular being analyzed as a multifractal object. Ophthalmologists can identify the regions where the specific damaged regions in retinopathy in diabetic patients are accurately differentiated.

Acknowledgements

The authors would like to thank Prof. Dr. Amal Elbendary Mansoura University ophthalmology center and in particular Dr. Mohamed Moawad Computer Engineering and Systems at Mansoura University Faculty of Engineering for their efforts.

References

[1] De Barros Garcia, David Leonrdo Cruvinel Isaac and Marcos Avila, (2017). Diabetic retinopathy and OCT angiography: clinical findings and future perspectives, International Journal of Retina and Vitreous, 3: 14: 2-10.

[2] Crawford TN, Alfaro DV 3rd, Kerrison JB, Jablon EP (2009) Diabetic retinopathy and angiogenesis. Curr Diabetes Rev 5: 8-13.

[3] Ye Sun and Lois E. H. Smith, Retinal Vasculature in Development and Diseases, (2018) Annu Rev Vis Sci.; 4: 101-122.

[4] Kostic M, Bates NM, Milosevic NT, Tian J, Smiddy WE, Lee W-H, Somfai GM, Feuer WJ, Shiffman JC, Kuriyan AE, Gregori NZ, Pineda S and Cabrera DeBuc D (2018) Investigating the Fractal Dimension of the Foveal Microvasculature in Relation to the Morphology of the Foveal Avascular Zone and to the Macular Circulation in Patients With Type 2 Diabetes Mellitus. Front. Physiol. 9: 1233. doi: 10.3389/fphys. 012334.

[5] Natasa Popovic, Mirko Lipovac, Miroslav Radunovic, Jurgi Ugarte, Erik Isusquiza, Andoni Beristain, Ramón Moreno, Nerea Aranjuelo, Tomo Popovic. (2019) Fractal characterization of retinal microvascular network morphology during diabetic retinopathy progression. Wiley Microcirculation journal, b DOI: 10.1111/micc.12531.

[6] Jirarattanasopa P, Ooto S, Tsujikawa A, et al. (2012) Assessment of macular choroidal thickness by optical coherence tomography and angiographic changes in central serous chorioretinopathy. Ophthalmology; 119: 1666–1678.

[7] Ohno-Matsui K, Akiba M, Moriyama M, et al. (2012) Acquired optic nerve and peripapillary pits in pathologic myopia. Ophthalmology.; 119: 1685–1692.

[8] Vasilios Katsikis, Methods for Biomedical Images. In "MATLAB - A Fundamental Tool for Scientific Computing and Engineering Applications - Vol. 3 (ed.) (2012), chapter 7, pp. 161-178.

[9] Mandelbrot B. B. (1991) Fractals and the rebirth of experimental mathematics. Fractals for the classroom, by H. O. Peitgen, H. Jurgens, D. saupe, E. M. Matelski, T. perciante, L. E. Yunker. New York: Springer, 1991.

[10] Ştefan Ţălu, Sebastian Stach, Dan Mihai Călugăru, Carmen Alina Lupaşcu, Simona Delia Nicoară, (2017) Analysis of normal human retinal vascular network architecture using multifractal geometry, Int J Ophthalmol, Vol. 10, No. 3, Mar. 18.

[11] Azemin MZ, Kumar DK, Wong TY, Kawasaki R, Mitchell P, et al. (2011) Robust methodology for fractal analysis of the retinal vasculature. IEEE Trans Med Imaging 30: 243-250.

[12] Mandelbrot, B. B. (1982), The Fractal Geometry of Nature, New York, W. H. Freeman, 95–107.

[13] Gould DJ, Vadakkan TJ, Poché RA, Dickinson ME (2011) Multifractal and lacunarity analysis of microvascular morphology and remodeling. Microcirculation 18: 136-151.

[14] D. Easwaramoorthy, P. S. Eliahim Jeevaraj, A. Gowrisankar, A. Manimaran and S. Nandhini, (2018). Fuzzy Generalized Fractal Dimensions Using Inter-Heartbeat Dynamics in ECG Signals far Age-Related discrimination, International Journal of Engineering & Technology, 7 (4.10) 900-903.

[15] R. Uthayakumar and A. Gowrisankar (2014) Generalized Fractal Dimensions in Image Thresholding Technique. Information Sciences Letters an International Journal. Inf. Sci. Lett. 3, No. 3, 125-134.

[16] Stosic T, Stosic BD (2006) Multifractal analysis of human retinal vessels. IEEE Trans Med Imaging 25: 1101-1107.

[17] Barabási AL, Vicsek T (1990) Self-similarity of the loop structure of diffusion-limited aggregates. J Phys A: Math Gen 23: L729-L733.

[18] Lopes R., Betrouni N., (2009) Fractal and multifractal analysis: A review. Medical Image Analysis, 13: 634–649.

[19] Posadas AND, Giménez D, Quiroz R, Protz R (2003) Multifractal characterization of soil pore systems. Soil Sci Soc Am J 2003, 67: 1361-1369.

[20] Zahid S, Dolz-Marco R, Freund KB, et al. Fractal dimensional analysis of optical coherence tomography angiography in eyes with diabetic retinopathy. Invest Ophthalmol Vis Sci. 2016; 57: 4940– 4947. DOI: 10.1167/iovs.16-19656.